American Journal of Modern Physics
2025, Vol. 14, No. 4, pp. 200-208
https://doi.org/10.11648/j.ajmp.20251404.14

Research Article

Electron Mobility in Single-layer Graphene

Konstantin Leonidovich Kovalenko, Sergei Ivanovich Kozlovskiy*, Nicolai Nicolaevich Sharan

Department of Sensor Systems, V. Lashkaryov Institute of Semiconductor Physics, National Academy of Sciences of Ukraine, Kyiv, Ukraine

Abstract

Analytical expressions for the low-field mobility of the two dimensional electrons in mono layer graphene are obtained on base of quantum kinetic approach that is based on the one-particle density matrix and the model non-equilibrium distribution function in form of the shifted Fermi distribution. We consider the gated graphene with the Fermi level that is biased by applying an external voltage to the gate. In this case, the confining potential has the shape of a triangle well that can be written in terms of Airy functions. Screened acoustic, optic phonons and ionized impurities are considered as scattering mechanisms. Calculations show that in the semiconductors with Dirac spectrum of charge carriers mobility for scattering by acoustic phonons and ionized impurities does not depend on the electron effective mass. Both effective mass of electrons and scattering rate by non-polar optic phonons reach minimum for electron energy close to the Dirac point. A comparison of the temperature dependences of the calculated and experimental mobility data shows that in the temperature range under consideration, at $T < 400$ K mobility is determined by the scattering of electrons by ionized impurities. The acoustic and out-of-plane optical phonons (ZO phonons) determine the electron mobility at higher temperatures. Results of mobility calculations are compared with known experimental data.

Keywords

Mobility, Mono Layer Graphene, Acoustic, Out-of-plane Optic Phonons, Ionized Impurities

1. Introduction

A theoretical understanding of two-dimensional material such as monolayer graphene is critical to determining their future uses and unlocking their properties. The unique electrical properties of graphene, such as high carrier mobility $2\times10^5 cm^2/V\,\text{sec}$ at room temperature offer significant advantages for applications ranging from fast electronics to touch screens and ultrasensitive photon detection [1, 2]. This mobility value can be strongly reduced by impurity and phonon scattering. Various theoretical approaches have been proposed to calculate the effect of impurities [1, 3] and acoustic phonons [3-6] on the carrier mobility in monolayer graphene. Among them are the relaxation time approximation (RTA) [3-7], numerical solution of the semi classical Boltzmann equation [8], Monte Carlo simulation [9-11].

Compared to analytical methods, the numerical solution process simulation is not always physically transparent and can be computationally intensive. The calculation results in this case are only valid within the range of the underlying data set. In the RTA the collision integral in the Boltzmann

*Corresponding author: lab25@isp.kiev.ua (Sergei Ivanovich Kozlovskiy)

Received: 26 June 2025; **Accepted:** 18 July 2025; **Published:** 31 July 2025

transport equation is modelled by a simple form which contains scalar relaxation time. For nanoscale transport the RTA give rise to some doubts for qualitative consideration of a wide circle of problems [12-14]. The problem of the mobility calculation in the RTA is to determine relaxation time for inelastic scattering process such as scattering by non-polar optic phonons. In the general case, the relaxation time for inelastic scattering cannot be introduced [15, 16].

In this article we derived analytic expressions for low field mobility monolayer graphene. Acoustic deformation potential, polar optical phonons and ionized impurities are adopted as scattering mechanisms. To calculate mobility we use the quantum kinetic approach that is based on the one-particle density matrix and the model non-equilibrium distribution function in form of the shifted Fermi distribution. The calculation results are compared with known experimental data.

2. Basic Equations

2.1. Dispersion Law

The dispersion law for electrons in graphene can be written as [8, 17].

$$\varepsilon_{\vec{k}} = \hbar V_F \left|\vec{k}_\perp\right|, \tag{1}$$

$V_F = 10^6$ m/sec is the Fermi velocity, $\vec{k}_\perp \in \{k_x, k_y\}$ is the wave vector, $\hbar$ is the reduced Plank constant.

Below we consider gated graphene with the Fermi level that is biased by applying some external voltage to the gate. In this case, the confining potential has the shape of a triangle well that can be written in terms of Airy functions $Ai(z)$ [18].

$$Ai(z) = \frac{1}{\pi}\int_0^\infty \cos\left(\frac{t^3}{3} + zt\right)dt, \tag{2}$$

where z is the direction of quantum confinement.

The energy Eigen values are

$$\varepsilon_l = L_E e E_{eff}\left(-a_l\right), \tag{3}$$

Here $L_E = \left(\hbar^2/2meE_{eff}\right)^{1/3}$ is characteristic length, E_{eff} is an effective surface field, e is the electron charge, a_n are zeros of the Airy functions that can be approximately given as [18].

$$a_l \cong -\left[\frac{3\pi}{2}\left(l - \frac{1}{4}\right)\right]^{2/3}, \quad l = 1, 2, \ldots \tag{4}$$

l is the quantum number.

If Fermi-level is shifted by applying of some bias voltage U the effective mass of electrons near the Dirac point can be written as [8].

$$m = \frac{\varepsilon_F}{V_F{}^2} = \frac{eU}{V_F{}^2}, \tag{5}$$

than $E_{eff} = U/L_z$ and expression for L_E takes a form

$$L_E = \left[\left(\frac{V_F\hbar}{\varepsilon_F}\right)^2 \frac{L_z}{2}\right]^{1/3} \tag{6}$$

L_z is the monolayer graphene thickness.

In this case the areal charge carrier density $n^{(D=2)}$ can be obtained by integration

$$n^{(D=2)} = \frac{2g}{(2\pi)^2}\sum_{l=1}\int \frac{d^2\vec{k}_\perp}{\exp\left[\varepsilon_{\vec{k}_\perp}/k_BT - \eta_l\right]+1} \tag{7}$$

$$\eta_l = \frac{\varepsilon_F - \varepsilon_l}{k_BT} = \frac{\hbar V_F k_F - \varepsilon_l}{k_BT} \tag{8}$$

g is the valley degeneracy, for graphene $g = 2$.

Integration (7) with dispersion law (1) gives

$$n^{(D=2)} = \frac{2}{\pi}\left(\frac{k_BT}{\hbar V_F}\right)^2 \sum_{l=1} F_1\left(\eta_l\right). \tag{9}$$

Here $F_r(\eta)$ are the Fermi-Dirac integrals

$$F_r(\eta) = \frac{1}{\Gamma(r+1)}\int_0^\infty \frac{x^r dx}{\exp(x-\eta)+1} \tag{10}$$

For high degeneration $\eta >> 1$

$$F_r(\eta) = \frac{\eta^{r+1}}{\Gamma(r+2)} \tag{11}$$

2.2. Quantum Kinetic Approach to Mobility Calculations

To compute the charged carrier mobility we will use the quantum kinetic approach [19-21] that is based on the one particle density matrix and the model non-equilibrium distribution function in form of the shifted Fermi distribution. In this case the model non-equilibrium distribution function is a solution of the quantum kinetic equation linearized with respect to

the electric field. For further consideration it is convenient to introduce the kinetic tensor that $\hat{\lambda}^{(D=2)}$ is the inverse mobility tensor $\hat{\lambda}^{(D=2)} = \left(\hat{\mu}^{(D=2)}\right)^{-1}$. For isotropic effective mass the kinetic tensor $\lambda^{(D=2)}$ degenerates into a scalar form. In the low-field limit the inverse mobility of carriers with dimensionality $D=2$ has the following form [19].

$$\lambda^{(D=2)} = -\frac{e\hbar}{(2\pi)^4 n^{(D=2)} k_B T}\int \frac{d\omega}{\sinh\left(\hbar\omega_{\vec{q}}/k_B T\right)}\int \vec{q}_\perp{}^2 < \varphi^2 >^{(D=2)}_{\omega,\vec{q}_\perp} d^2\vec{q}_\perp \int d^2\vec{k}_\perp \left(f^0_{\vec{k}_\perp} - f^0_{\vec{k}_\perp - \vec{q}_\perp}\right)\delta\left(\varepsilon_{\vec{k}_\perp} - \varepsilon_{\vec{k}_\perp - \vec{q}_\perp} \mp \hbar\omega_{\vec{q}_\perp}\right)\Phi\left(\varepsilon_{\vec{k}_\perp} - \hbar\omega_{\vec{q}_\perp}\right) \quad (12)$$

$f^0_{\vec{k}_\perp}$ is the Fermi equilibrium distribution function, k_B is the Boltzmann's constant, T is temperature, $\langle\varphi^2\rangle^{(D)}_{\omega,\vec{q}_\perp}$ is the spectral correlator of scattering potential.

We will assume that in scattering process a charged carrier makes transition from some initial state $\vec{k}_\perp(k_x,k_y)$ into the final state $\vec{k}'_\perp = \vec{k}_\perp - \vec{q}_\perp$, thus $\hbar\vec{q}_\perp$ is the transferred momentum, $\varepsilon_{\vec{k}_\perp} - \varepsilon_{\vec{k}_\perp - \vec{q}_\perp} = \pm\hbar\omega_{\vec{q}_\perp}$ is the change in energy at collision. The upper sign in argument of the Dirac delta function in (12) is used for phonon emission and the lower sing is used for phonon absorption. $\Phi\left(\varepsilon_{\vec{k}_\perp} - \hbar\omega_{\vec{q}_\perp}\right)$ is the Heaviside step function that ensures a positive kinetic energy of electrons for scattering with emission of phonons (primarily for non-polar optic phonons). The scattering by acoustic phonons and ionized impurities we will consider as elastic ($\omega, \omega_{\vec{q}_\perp} \to 0$).

2.2.1. Correlator for Scattering 2DEG by Acoustic and Non-polar Optic Phonons

Correlators for 2DEG for scattering on acoustic phonons we obtain from correlator for 3DEG $\langle\varphi^2\rangle^{(D=3)}_{\omega,\vec{q}}$ by the inverse Fourier transform. The correlators for 3DEG scattering on by acoustic and non-polar optic phonons [19-22] are

$$\langle\varphi_{Ac}{}^2\rangle^{(D=3)}_{\omega,\vec{q}} = \left(\frac{\Xi}{e}\right)^2 \frac{\pi\hbar\omega}{2\rho s_L{}^2}\coth\left(\frac{\hbar\omega}{2k_B T}\right)\left[\delta(\omega - s_L q) + \delta(\omega + s_L q)\right], \quad (13)$$

$$\left\langle\varphi^2{}_O\right\rangle^{(D=3)}_{\omega,q} = \left(\frac{D}{e}\right)^2 \frac{\pi\hbar}{2\rho\omega_0}\coth\left(\frac{\hbar\omega_0}{2k_B T}\right)\left[\delta\left(\omega - \omega_0\right) + \delta\left(\omega + \omega_0\right)\right], \quad (14)$$

where Ξ and D are the deformation potential coupling constants, $\hbar\omega_0 = E_{DO}$ is energy of non-polar optic phonon, ρ and s_L are density of the crystal and velocity of the longitudinal acoustic phonon, respectively. Acoustic phonon scattering is treated within the elastic deformation potential approach in the long-wavelength acoustic-phonon limit.

The inverse Fourier transform gives the correlator for the 2DEG associated with the plane $z=0$ as follows:

$$\langle\varphi^2\rangle_{\omega,\vec{q}_\perp}{}^{(D=2)} = \frac{1}{2\pi}\int_{-\infty}^{\infty}\left\langle\varphi^2\right\rangle_{\omega,\vec{q}}{}^{(D=3)}\left|F_{ll'}\left(q_z\right)\right|^2 dq_z . \quad (15)$$

Here $\vec{q}_\perp\left(q_x,q_y\right)$ and $\vec{q}\left(q_x,q_y,q_z\right)$ are the wave vectors for 2DEG and 3DEG, respectively.

The fundamental difference between 2DEG and 3DEG is the overlap integral, which determines the effective extent of The inverse Fourier transform gives the correlator for the 2DEG associated with the plane $z=0$ as follows:

$$F_{ll'}\left(q_z\right) = \int_0^\infty \exp(-iq_z z)\,\xi_l\left(z\right)\xi_{l''}\left(z\right)dz . \quad (16)$$

Here $\xi_l\left(z\right)$ and $\xi_{l'}\left(z\right)$ are the envelope functions in the confined direction

$$\xi_{l(l')}(z) = \frac{1}{\sqrt{L_E A I_{l(l')}}}\,Ai\left(\frac{z}{L_E} + a_{l(l')}\right), \quad (17)$$

$$I_{l(l')} = \sqrt{\int_0^\infty\left[Ai\left(y + a_{l(l')}\right)\right]^2 dy} \quad (18)$$

Finally we have

$$F_{ll'}(q_z)=\frac{1}{\sqrt{I_l I_{l'}}}\int_0^\infty dy\exp\left(-iq_z L_E y\right)Ai\left(y+a_l\right)Ai\left(y+a_{l'}\right) \tag{19}$$

Integration (15) gives the following expression for correlators

$$\langle\varphi_A{}^2\rangle_{q_\perp,\omega}^{(D=2)}=\left(\frac{\Xi}{e}\right)^2 A_{ll'}S_R^{(D=2)}\left(q_\perp,q_0\right)\frac{\pi\hbar\omega^2}{2\rho s_L{}^2}\coth\left(\frac{\hbar|\omega|}{2k_BT}\right), \tag{20}$$

$$\left\langle\varphi_O{}^2\right\rangle_{\omega,\vec{q}_\perp}^{(D=2)}=\left(\frac{D_0}{e}\right)^2\frac{A_{ll'}\pi\hbar}{2\rho\omega_0 L_E}S_R^{(D=2)}\left(q_\perp,q_0\right)\coth\left(\frac{\hbar\omega_0}{2k_BT}\right)\left[\delta(\omega-\omega_0)+\delta(\omega+\omega_0)\right] \tag{21}$$

Here

$$A_{ll'}=\frac{1}{2\pi I_l I_{l'}}\int_{-\infty}^{\infty}dx\left|\int_0^\infty\exp\left(-ixy\right)Ai\left(y+a_l\right)Ai\left(y+a_{l'}\right)dy\right|^2 \tag{22}$$

$S_R^{(D=2)}\left(q_\perp,q_0\right)$ is the screening factor and $A_{11}=0.417$, $A_{12}=0.158$, $A_{22}=0.291$, $A_{23}=0.135$.

$$S_R^{(D=2)}\left(q_\perp,q_0\right)=q_\perp{}^2\Big/\left(q_\perp+q_0\right)^2, \tag{23}$$

q_0 is the inverse characteristic screening length.

For carriers with Dirac like dispersion law (1) the inverse characteristic screening length can be found by differentiation [21].

$$q_0=\frac{2\pi e^2}{k_BT\kappa}\frac{\partial n^{(D=2)}}{\partial\eta}=\frac{4e^2k_BT}{\pi\kappa\left(\hbar V_F\right)^2}\ln\left[1+\exp(\eta)\right]. \tag{24}$$

$\kappa=4\pi\varepsilon_0\varepsilon_b$ is the dielectric permittivity, ε_0 and ε_b are the vacuum and relative background dielectric constants, respectively.

2.2.2. Impurity Scattering

At scattering by ionized impurities the spectral correlator is given by [19].

$$\langle\varphi_I{}^2\rangle_{\omega,q_\perp}{}^{(D=2)}=\frac{\left(2\pi\right)^3e^2N_I^{(D=2)}}{\varepsilon_L{}^2q_\perp{}^2}A_{ll'}^{(I)}\left(q_\perp\right)^2S_R^{(D=2)}\left(q_\perp,q_0\right)\delta\left(\omega\right), \tag{25}$$

$N_I^{(D=2)}$ is areal density of scattering centres.

In this case, the overlap integral can be written as [22].

$$A_{ll'}^{(I)}(q_\perp)=\frac{1}{I_lI_{l'}}\int_0^\infty\exp\left(-|\vec{q}_\perp|L_Ey\right)Ai\left(y+a_l\right)Ai\left(y+a_{l'}\right)dy \tag{26}$$

In the long wave approximation $q_\perp\to0$ the overlap integral takes a form

$$A_{ll'}^{(I)}(q_\perp)\approx\delta_{ll'}\exp\left(-2q_\perp L_E\right). \tag{27}$$

2.3. Mobility of 2DEG with Dirac Spectrum

2.3.1. Scattering by Acoustic Phonons

For scattering by acoustic phonons integration (12) with correlator gives expression for inverse mobility in the following form

$$\left(\mu_{Ac}^{(D=2)}\right)^{-1}=\lambda_{Ac}{}^{(D=2)}=\left(\frac{\Xi}{e}\right)^2\frac{eA_{ll'}}{8F_1\left(\eta\right)\rho s^3}\frac{\left(k_BT\right)^4}{\left(\hbar V_F\right)^4}\int_0^\infty\frac{x^6}{\left(x+x_0\right)^2}\left(-\frac{\partial f^0\left(\eta\right)}{\partial x}\right)dx \tag{28}$$

where

$$x_0 = q_0\left(\frac{\hbar V_F}{k_B T}\right) = \frac{4e^2}{\varepsilon_L(\hbar V_F)}\ln\left[1+\exp(\eta)\right]. \quad (29)$$

In neglect screening $x_0 << 1$ expression for mobility can be written as

$$\mu_{Ac}^{(D=2)} = \frac{2\rho s^3}{3(\Xi/e)^2 A_{ll'} e}\left(\frac{\hbar V_F}{k_B T}\right)^4 \frac{F_1(\eta)}{F_3(\eta)}. \quad (30)$$

For non-degenerated electrons $\eta << -1$

$$F_1(\eta)/F_3(\eta) = 1. \quad (31)$$

The temperature dependence of mobility (30) goes as $\mu_{Ac}^{(D=2)} \propto T^{-4}$ without screening effects. This dependence was obtained earlier [3, 7].

For strong degeneration $\eta >> 1$ expression for mobility simplifies

$$\mu_{Ac}^{(D=2)} = \frac{8\rho s^3}{\pi(\Xi/e)^2 A_{ll'} e n^{(D=2)}}\left(\frac{\hbar V_F}{k_B T}\right)^2. \quad (32)$$

In this case, mobility decreases with increasing electron density.

2.3.2. Scattering by Non-polar Optic Phonons

For scattering by non-polar optic phonons integration (12) with (21) gives

$$\left(\mu_O^{(D=2)}\right)^{-1} = \lambda_O^{(D=2)} = \left(\frac{D_0}{e}\right)^2\left(\frac{k_B T}{\hbar V_F}\right)^4 \frac{A_{ll'} e\hbar^3 F(x, x_{DO}, \eta)}{32F_1(\eta)(k_B T)^3 \sinh^2\left(\frac{x_{DO}}{2}\right)\rho L_E x_{DO}}, \quad (33)$$

where

$$F(x, x_{DO}, \eta) = \int_0^\infty x\left(x^2 + (x+x_{DO})^2\right)(x+x_{DO})dx \times S_R(x, x_{DO}, \eta)\left[\frac{1}{\exp(x-\eta)+1} - \frac{1}{\exp(x+x_{DO}-\eta)+1}\right]. \quad (34)$$

Here screening factor $S_R(x, x_{DO}, \eta)$

$$S_R(x, x_{DO}, \eta) = \int_0^{2\pi} d\varphi_k \int_0^{2\pi} d\varphi_Q \frac{(x+x_{DO})^2 + x^2 - 2(x+x_{DO})x\cos(\varphi_k - \varphi_Q)}{\left[\sqrt{(x+x_{DO})^2 + x^2 - 2(x+x_{DO})x\cos(\varphi_k - \varphi_Q)} + 2x_{DO}\right]^2}, \quad (35)$$

$x_{DO} = E_{DO}/k_B T$ is the normalized energy of the non-polar optic phonons.

The higher mobility of electrons can be reached at low electron densities. In this case we can neglect by screening $x_{DO} << 1$, $S_R(x, x_{DO}, \eta) = 1$ and expression (34) is significantly simplified.

2.3.3. Impurity Scattering

For scattering by ionized impurities the components of the kinetic tensor can be obtained by integration (12) with correlator (25).

$$\lambda_I^{(D=2)} = \frac{\pi^2 e^3 N_I^{(D=2)}}{\kappa^2 \hbar V_F^2 F_1(\eta)} \int_0^1 \frac{F_{ll'}(x,z)^2 z^2}{(xz+x_0)^2\sqrt{1-z^2}} dz \int_0^\infty \frac{\partial f_0}{\partial x} x^3 dx. \quad (36)$$

$$F_{ll'}(x,z) \approx \delta_{ll'} \exp\left(-4xz\frac{k_B T}{\hbar V_F} L_E\right). \quad (37)$$

In neglect screening

$$\lambda_I^{(D=2)} = \frac{\pi^2 e^3 N_I^{(D=2)}}{\varepsilon_L^2 \hbar V_F^2 F_1(\eta)} \int_0^1 \frac{F_{ll'}(x,z)^2}{\sqrt{1-z^2}} dz \int_0^\infty \frac{\partial f_0}{\partial x} x^2 dx. \quad (38)$$

For mixed scattering when electrons are scattered by acoustic $\lambda_{Ac}^{(D=2)}$, non-polar optic $\lambda_O^{(D=2)}$ phonons and ionized impurities $\lambda_I^{(D=2)}$

$$\lambda_{mix}^{(D=2)} = \lambda_{Ac}^{(D=2)} + \lambda_O^{(D=2)} + \lambda_I^{(D=2)} \quad (39)$$

The mobility value can be found by summing over the quantum numbers of the reduced Fermi energy η_l (8) given by

$$\mu^{(D=2)} = \frac{\sum_{l,l'} n^{(D=2)}(\eta_l) / \lambda_{mix}{}^{(D=2)}(\eta_l)}{\sum_{l} n^{(D=2)}(\eta_l)}. \qquad (40)$$

The summation is carried out until the mobility ceases to depend on the quantum numbers.

3. Discussion

In this section we compare results of our calculations with known experimental data of the low-field mobility in the single-layer graphene. In these calculations we used the following values of the material constants: the longitudinal sound velocity is $s = 2\times10^4$ m/sec [7, 23], single layer graphene thickness $L_z = 1nm$ [24] and mass density $\rho = 7.6$ g/cm^3 [9], relative dielectric constant $\varepsilon_b = 5.7$ [17]. The value of coupling constants for scattering by non-polar optic phonon in our calculations is adopted $D_O = 10^{10} eV/cm$. The coupling constants for scattering by acoustic Ξ and Non-Polar optic phonons energy E_{DO} are considered as fitting parameters.

Experimental (circles) [25-28] and calculated (solid lines) temperature dependences of the resistivity and electron mobility for different values of the energy of optical phonons in single-layer graphene are shown in Figures 1-3. The value of the acoustic coupling constant $\Xi = 14eV$ used in calculations are in the range obtained previously [4, 7].

The phonon spectrum in single-layer graphene has been studied in detail [29-32]. The calculated phonon dispersion includes optical phonons with the two main modes: longitudinal optical phonons (LO) and out-of-plane optical phonons (ZO) with energies approximately (meV) 200 and 100, respectively. A comparison of the calculated and experimental temperature dependences of electron mobility in Figures 1-3 shows that the energies of optical phonons are significantly lower than the known values for LO phonons and are close to the energies for ZO phonons. Thus, electron mobility at high temperatures T> 200K is limited by electron scattering on ZO phonons.

Experimental and calculated temperature dependences of electron mobility in single-layer graphene are shown in Figure 2. The contribution of different scattering mechanisms to the electron mobility is shown in the inset to Figure 2. At temperatures T< 400K mobility is determined by the scattering of electrons on ionized impurities. At higher temperatures, scattering by optic and acoustic phonons predominates. In this case, the contribution of acoustic phonons is relatively small.

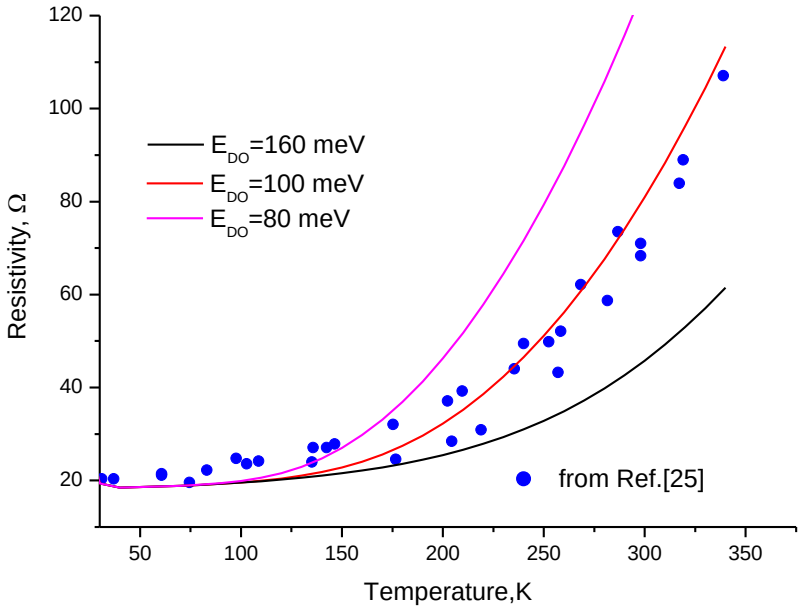

Figure 1. *Experimental (circles) [25] and calculated ($N_I{}^{(D=2)} = 2\times10^{12} cm^{-2}$, $\Xi = 14eV$) (solid lines) temperature dependences of resistivity single-layer graphene are shown for different values of optic phonon energies E_{DO}.*

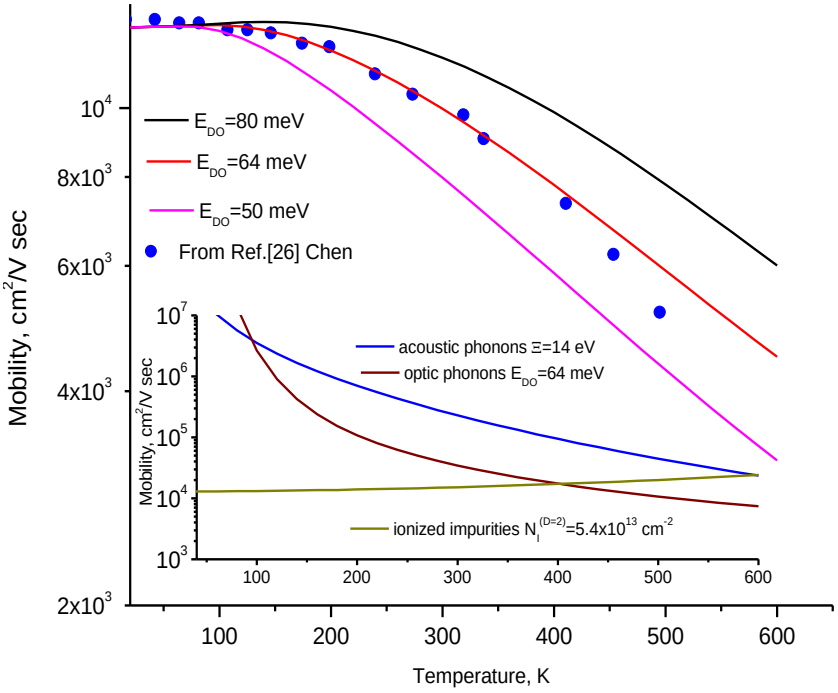

Figure 2. *Experimental (circles) [26] and calculated ($\Xi = 14\,eV$, $N_I^{(D=2)} = 5.4\times10^{13} cm^{-2}$) (solid lines) temperature dependences of mobility are shown for different values of the optic phonon energy E_{DO}. The inset shows the contribution of different scattering mechanisms to temperature dependence of electron mobility.*

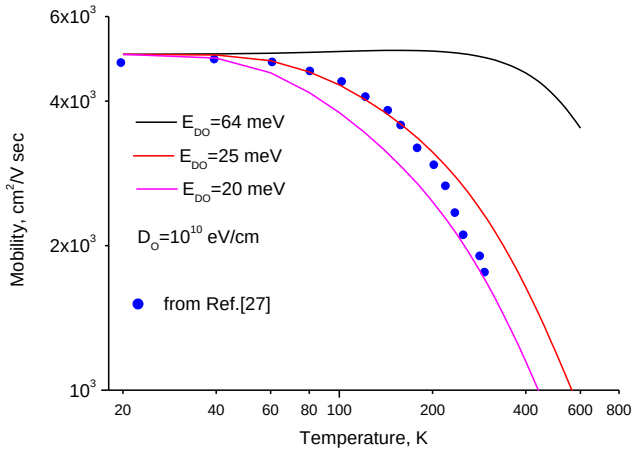

Figure 3. *Experimental (circles) [27] and calculated ($\Xi = 14\,eV$, $N_I^{(D=2)} = 1.4\times10^{14} cm^{-2}$) (solid lines) temperature dependences of mobility are shown for different energies of Non-Polar optic phonons E_{DO}.*

Experimental [27] and calculated dependences of mobility on electron density in single-layer graphene are shown in Figure 4. The sharp increase in electron mobility with electron density less $2\times10^{11} cm^{-2}$ is striking. This increase is due to the peculiarity of electron scattering on non-polar optic phonons. As it follows from (33) mobility for non-polar optic phonon scattering is proportional to L_E which decreases with electron energy close to Dirac point where the electron effective mass $m \to 0$ [8]. Thus, at high temperatures and low electron densities, scattering by optical phonons decreases, and electron mobility is determined by acoustic phonon scattering. As follows from (28) and (36), the electron mobility for both scattering by acoustic phonons and ionized impurities does not depend on the effective electron mass.

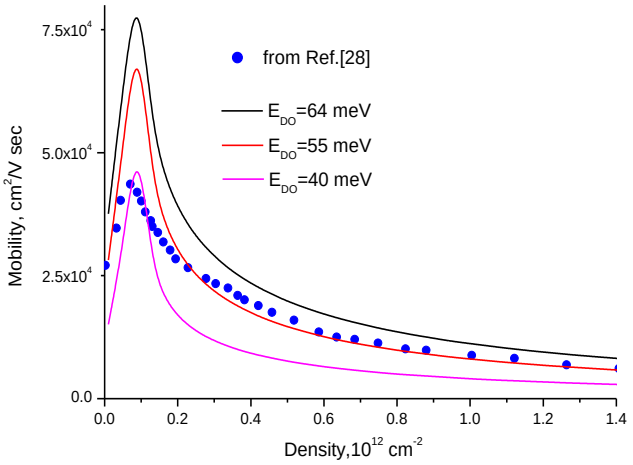

Figure 4. *Experimental (circles) [28] and calculated (solid lines) dependences of mobility on electron density in single-layer graphene are shown at 300K for different values for different values of the optic phonon energy E_{DO}.*

4. Conclusion

In summary, we have carried out a systematic theoretical study of the low-field mobility of the two dimensional electron gas in single layer graphene. Analytical expressions for mobility during scattering by acoustic, non-polar optical phonons and ionized impurities are obtained. A feature of the two-dimensional gas with the Dirac spectrum is that the mobility of electrons for scattering by acoustic phonons and ionized impurities does not depend on the electron effective mass. The scattering by optic phonons reaches minimum for electron energy close to Dirac point. In the temperature range under consideration, at $T < 400K$ mobility is determined by the scattering of electrons on ionized impurities. Acoustic and out-of-plane optical phonons (ZO phonons) determine the electron mobility at higher temperatures. The calculated temperature and carrier density dependences of electron mobility in single layer grapheme under consideration are in agreement with known experimental data.

Author Contributions

Sergei Ivanovich Kozlovskiy: Formal Analysis, Funding acquisition, Investigation, Project administration, Validation, Visualization

Konstantin Leonidovich Kovalenko: Conceptualization, Funding acquisition, Methodology, Project administration, Resources, Supervision, Validation, Writing - original draft, Writing - review & editing

Nicolai Nicolaevich Sharan: Conceptualization, Formal Analysis, Methodology, Project administration, Software, Visualization, Writing - review & editing

Data Availability Statement

The data that supports the findings of this study are available within the article Author Declarations.

Conflicts of Interest

The authors declare no conflicts of interest.

References

[1] J. H. Gosling. O. Makarovsky, F. Wang, et al. Commun Phys 4 30(2021).

[2] W. Zhu, V. Perebeinos, M. Freitag, and P. Avouris Phys. Rev. B 80 235402 (2009).

[3] I. I. Boiko Semiconductor Physics, Quantum Electronics & Optoelectronics 15 129(2012).

[4] K. V. Nguyen and Y. Chang Phys. Chem. Chem. Phys. 22 3999 (2020).

[5] S. H. Mir, V. K. Yadav and J. K.. Singh. ACS Omega 5 14203 (2020).

[6] S. Das Sarma, S. Adam, E. H Hwang, and E. Rossi Rev. Mod. Phys. 83 407(2011).

[7] E. H. Hwang, S. Das Sarma Phys. Rev. B 77 115449 (2008).

[8] A. H. Castro Neto, F. Guinea, N. M. R Peres, K. S. Novoselov, and. A. K. Geim Rev. Mod. Phys. 81 109(2009).

[9] D. Smith and L. von Smekal Phys. Rev. B 89 195429 (2014).

[10] A. Majorana, G. Mascali, and V. Romano Journal of Mathematics in Industry 7 4(2017).

[11] A. Akturka, and N. Goldsman J. Appl. Phys. 103 053702 (2008).

[12] H. Hirai, H. Tsuchiya, Y. Kamakura, N. Mori, and M. Ogawa Journal of Applied Physics 116 083703 (2014).

[13] T. Grasser, H. Kosina, S. Selberherr. In: Wachutka, G., Schrag, G. (eds) Simulation of Semiconductor Processes and Devices 2004. Springer, Vienna.

[14] V. Chiloyan, S. Huberman, Z. Ding, J. Mendoza, A. A. Maznev, K. A. Nelson, and G. Chen Phys. Rev. B 104 245424 (2021).

[15] G. Wilk, Z. Włodarczyk. Eur. Phys. J. A 57 221(2021).

[16] B K Readly Quantum Processes in Semiconductors (Oxford University Press 2013).

[17] R. S. Shishir, F. Chen, J. Xia, N. J. Tao, D. K. Ferry J Comput Electron 8 43(2009).

[18] D. K. Ferry, S. M. Goodnick, and J. Bird Transport in Nanostructures. Cambridge University Press, Cambridge (2009).

[19] I. I. Boiko Kinetics of Electron Gas Interacting with Fluctuating Potential. (Naukova dumka, Kiev, 1993).

[20] K. L Kovalenko, S. I. Kozlovskiy, N. N. Sharan, E. F. Venger J. Phys.: Condens. Matter 36 325705 (2024).

[21] K. L Kovalenko, S. I, Kozlovskiy, and N. N. Sharan AIP Advances 15 035156 (2025).

[22] K. L Kovalenko, S. I Kozlovskiy, and N. N. Sharan J Comput Electron 17 926(2018).

[23] X. Cong, Q. Q. Li, X. Zhang, M.-L. Lin, J. B. Wu, X. L. Liu, P. Venezuela, P. H. Tan Carbon 149, 19-24 (2019).

[24] C. J. Shearer, A. D. Slattery J Stapleton Andrew, Shapter and Gibson C. T. Nanotechnology 27 125704 (2016).

[25] S. V Morozov., K. S Novoselov, M. I Katsnelson, F. Schedin, D. C. Elias., J. A Jaszczak., and A. K.. Geim Phys. Rev. Lett. 100 01660 (2008).

[26] Chen J. H., Jang C., Xiao S., Ishigami M. and Fuhrer M. S. Nature Nanotech 3 206(2008).

[27] Tiras E., Ardali S., Tiras T., Arslan E., Cakmakyapan S., Kazar O., Hassan J., Janzen E., and Ozbay E. J. Appl. Phys. 113 04370 (2013).

[28] R. S. Shishir and D. K. Ferry J. Phys.: Condens. Matter 21 232204 (2009).

[29] D. L. Nika, E. P., Pokatilov and A. A. Balandin Phys. Status Solidi B 248 2609 (2011).

[30] A Politano, F de Juan, G Chiarello, and H Fertig Physical Review Letters 115 075504 (2015).

[31] A. A. Taleb, D. J. Far ás Phys.: Condens. Matter 28 103005 (2016).

[32] B. Hellsing, T, Frederiksen Phys. Rev. B 110 155426 (2024).